THE ASTROPHYSICAL JOURNAL, 494:381–395, 1998 February 10

THE *ASCA* X-RAY SPECTRUM OF η CARINAE

M. F. CORCORAN,[1] R. PETRE, J. H. SWANK, AND S. A. DRAKE[1]
Laboratory for High Energy Astrophysics, Goddard Space Flight Center, Greenbelt MD 20771;
corcoran@barnegat.gsfc.nasa.gov

K. KOYAMA AND Y. TSUBOI
Department of Physics, Faculty of Science, Kyoto University, Sakyo-ku, Kyoto 606-01, Japan

R. VIOTTI
Instituto Astrofisica Spaziale, CNR, Via E. Fermi 21, 1-00044 Frascati, RM, Italy

A. DAMINELI[2]
Instituto Astronomico e Geofisico da USP, CP 9638, 01065-970 Sao Paulo, Brazil

K. DAVIDSON AND K. ISHIBASHI
Department of Astronomy, University of Minnesota, 116 Church Street, SE, Minneapolis, MN 55455

AND

S. WHITE AND D. CURRIE
Department of Physics and Astronomy, University of Maryland, College Park, MD 20742
Received 1997 April 30; accepted 1997 September 19

ABSTRACT

We have obtained high signal-to-noise ratio 0.5–10 keV band X-ray spectra of the peculiar, extremely luminous star η Carinae with the *Advanced Satellite for Cosmology and Astrophysics* (*ASCA*) X-ray observatory during Cycle 4 observations in mid-1996. These data comprise the best X-ray spectra to date of the cool source ($kT \sim 0.3$ keV) surrounding the homunculus and of the hot source ($kT \sim 5$ keV) associated with η Car itself. We identify line emission from ions of N, Mg, Si, and S and numerous strong transitions of Fe in a variety of ionization stages, including the first clear identification of a fluorescent Fe line produced by photoionization of cool material by the X-ray continuum from the hot source. The line strengths are consistent with thermal equilibrium models, though abundances of some important elements are nonsolar. Our analysis suggests that Fe is slightly underabundant and S and Si somewhat overabundant. Most importantly, we confirm the high N enrichment derived by Tsuboi et al. from their analysis of a shorter *ASCA* observation obtained during the performance verification (PV) phase in 1993 August. The O/N abundance ratio derived from the *ASCA* spectra is consistent with an upper limit from optical/UV spectral analysis (Davidson et al.) and with predictions of evolutionary models for extremely massive stars. Comparison of the Cycle 4 and PV-phase spectra shows that the X-ray luminosity increased by $\sim 50\%$ during this 3 year interval. Using the *ASCA* spectral model as a template, we reevaluate the spectrum of η Car obtained by the *Röntgen Satelite* (*ROSAT*) in late 1992 and construct an X-ray light curve for the 1992.4–1996.6 interval. We present spectra from the *International Ultraviolet Explorer* (*IUE*) satellite obtained at nearly the same time as the Cycle 4 *ASCA* spectra and show that the observed X-ray variability is reflected in changes of some important UV spectral features. Our data suggest that the X-ray emission and state of the stellar wind are intimately connected, though the exact mechanism of coupling is not known. We suggest two alternatives: an underlying photospheric change of undetermined origin in η Car itself, or a collision between a dense stellar wind from η Car and the wind or photosphere of a companion.

Subject headings: stars: abundances — stars: individual (η Carinae) — stars: early-type — X-rays: stars

1. INTRODUCTION

The peculiar star η Carinae has been called the most massive and luminous star known (van Genderen & Thè 1984; Davidson 1987, 1989). During the "Great Eruption" in the 1840s, η Car expelled $\geq 1\ M_\odot$ of gas (Andriesse, Donn, & Viotti 1978) and became for a while the second brightest star. The expelled gas forms a beautiful $12'' \times 17''$ bipolar dusty nebula, the "homunculus" (Gaviola 1950; Walborn 1976; Hester et al. 1991; Morse 1996; Currie et al. 1997), which currently obscures the star from direct view. Despite intense interest and more than 150 years of detailed photometric, spectrophotometric, astrometric, interferometric, and polarimetric observation, the nature of the eruption (and the star) is still a matter of some controversy.

η Car is a strong X-ray source; characteristically, its X-ray emission is quite distinct, compared to that of other normal, well-studied, X-ray–bright stars (for example, ζ Ori and ϵ Ori, Cassinelli & Swank 1983; ζ Puppis, Corcoran et al. 1993; δ Ori and λ Ori, Corcoran et al. 1994b; β Ceti and π^1 UMa, Drake et al. 1994; λ Eri, Smith et al. 1997). Observations with the Imaging Proportional Counter (IPC), the High Resolution Imager (HRI), the Solid State Spectrometer (SSS), and the Monitor Proportional Counter (MPC) on the *Einstein Observatory* (Seward et al. 1979; Seward & Chlebowski 1982; Chlebowski et al. 1984) revealed a multicomponent thermal X-ray spectrum with characteristic temperatures of a few tenths of a keV and

[1] Universities Space Research Association, 7501 Forbes Boulevard, Suite 206, Seabrook, MD 20706.
[2] Joint Institute for Laboratory Astrophysics, Boulder, CO 80309.

more than 4 keV. Chlebowski et al. showed that the emission is spatially structured, consisting of a pointlike "knot" or "core" spatially coincident with the optical star surrounded by a large, elliptical, inhomogeneous "shell" extending some 0.5 pc from the star. They showed that, at energies above 3 keV, η Car was the only visible source in the IPC field and proposed the "core" as the source of the hard emission, with the cooler emission confined to the "shell." The *Einstein* images also showed numerous X-ray point sources near η Car (generally associated with the other massive stars in the region), as well as diffuse hot gas throughout the Carina Nebula.

Koyama et al. (1990) obtained a high signal-to-noise ratio spectrum of a $1^\circ \times 2^\circ$ region including η Car with the *Ginga* X-ray observatory. The *Ginga* spectrum provided the best measure to that time of the Fe line region near 7 keV. Analysis of the spectrum by Koyama et al. yielded a temperature near 4 keV for the hottest emission. Koyama et al. noted that the *Ginga* flux was larger than the scaled *Einstein* flux obtained by Chlebowski et al. and suggested contamination of the *Ginga* data by an additional source of hot flux (not associated with η Car) in the Carina Nebula.

ROSAT obtained spectrally and spatially resolved X-ray observations of the region around η Car with the Position Sensitive Proportional Counter (PSPC; Corcoran et al. 1995, hereafter CRSP) and the High Resolution Imager (Corcoran et al. 1996). The PSPC observations confirmed that the "core" was indeed the source of the hot flux, with cooler material located in the "shell." The PSPC observations revealed that the hot "core" component varied dramatically, increasing in brightness by a factor of 2 in only a 4 month interval, with no significant change in the extended diffuse emission. Analysis of the PSPC spectra was not able to constrain the combination of temperature, column density, and/or emission measure that gave rise to the observed change, owing to the low effective area of the instrument at $E \geq 2$ keV. However, the observed change was consistent with an increase in the emission measure of the hot component at constant temperature and column depth. Interestingly, changes in the 5 GHz radio continuum emission (Duncan et al. 1995) were seen near the time of the X-ray variations. The X-ray low state was also found to correspond temporally to a so-called shell event, i.e., an episode of low excitation marked by weak He I 10830 Å emission; such "shell events" have been shown to recur with a 5.52 yr period (Damineli 1996).

Tsuboi et al. (1997; hereafter TKSP) analyzed an X-ray spectrum obtained in 1993 with the Solid State Imaging Spectrometer (SIS) on the *ASCA* observatory. *ASCA* (Tanaka, Inoue, & Holt 1994; Serlemitsos et al. 1995) provides spatially resolved moderate-resolution X-ray spectrometry in the 0.5–10 keV band. Since the bulk of the X-ray emission from η Car falls in this band, and since η Car is a strong thermal source in a spatially crowded field, *ASCA* is well suited to study the η Car X-ray spectrum free of contamination from nearby sources. TKSP confirmed the variability reported by CRSP and also derived a large overabundance of nitrogen in the cool source. They derived an oxygen to nitrogen abundance ratio of ~ 0.2, a value much lower than the solar value (O/N = 7.6) but consistent with the low O/N ratio determined independently from observations at other wavelengths (Rodgers & Searle 1967; Davidson, Walborn & Gull 1982; Davidson et al. 1986). The low O/N abundance ratio can be interpreted in terms of CNO processing in an evolved, massive star (Davidson et al. 1982; TKSP).

To define better the properties of the X-ray spectrum, the elemental abundance in the X-ray-emitting gas, and the magnitude and nature of the X-ray variability, we obtained a deep X-ray spectrum of η Car with the *ASCA* SIS and Gas Imaging Spectrometer (GIS) detectors. This new observation is nearly a factor of 5 greater in exposure than the 1993 observation and thus allows more accuracy in determining temperatures and line strengths.

This paper is organized as follows. In § 2, we describe the *ASCA* observations and data reduction. In § 3, we present the GIS X-ray light curve of η Car and show that the star underwent no dramatic variation during the *ASCA* observation. In § 4, we discuss the extraction and fitting of the *ASCA* SIS and GIS spectra. We compare our results to earlier *ASCA* and *ROSAT* spectra in § 5 and use these data to derive the X-ray light curve of η Car in the interval 1992.4–1996.6. We present contemporaneous *IUE* spectra in § 6 and note variability in the strengths of some UV spectral features during the X-ray variations. We discuss the major points of our analysis in § 7, while conclusions and suggestions for future observational work are given in § 8.

2. *ASCA* CYCLE 4 OBSERVATION OF η CAR

The *ASCA* observation began on 1996 July 29 and spanned more than 200 ks with approximately 80 ks of good science time achieved in each instrument. *ASCA* has on board two SIS and two GIS instruments which simultaneously view the target. Table 1 lists the journal of observations for each instrument. Most of the data were obtained using high or medium telemetry rates. The SIS observations were obtained in 1 CCD mode; a single SIS CCD has a field of view of $11' \times 11'$. The GIS has a circular field of view of $50'$ diameter and so includes emission from the nearby sources WR 25 (=HD 93162), HD 93250, and the open cluster Tr 14.

We derived good X-ray events from the unfiltered processed *ASCA* data by excluding times of SAA passage and intervals when the Earth elevation angle was less than 5° for the GIS data and less than 10° (20° for bright Earth) for the SIS data. We also excluded times of low geomagnetic rigidity and times when the satellite pointing was more than $0.^\circ 01$ from the nominal position of η Car. SIS data were cleaned of events caused by "hot" and "flickering" CCD pixels, and the GIS data were cleaned of calibration source events and other background events based on rise time discrimination. We used corrected values of the above parameters when screening the data; the original parameter values provided by the *ASCA* Data Facility were incorrect owing to a processing problem affecting spacecraft orbit data in the 1996 July–1997 February interval.

We extracted images from the screened events using the XSELECT analysis software provided and maintained by

TABLE 1

ASCA CYCLE 4 OBSERVATIONS OF η CARINAE

Instrument	Start (JD −2,450,294)	Stop (JD −2,450,294)	Exposure (s)
SIS0	0.39	2.99	81,696
SIS1	0.35	2.92	80,385
GIS2	0.40	2.88	77,528

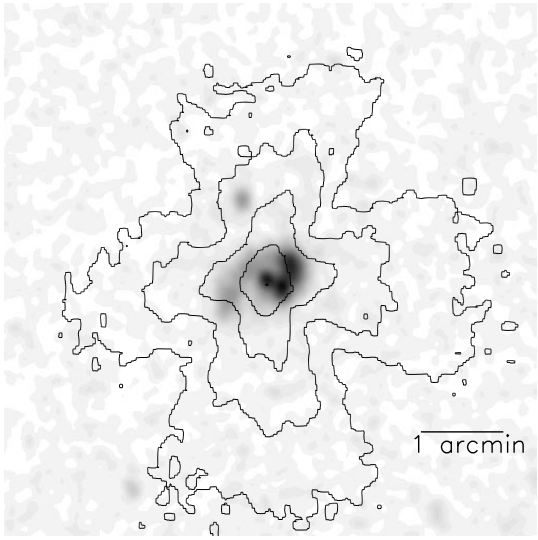

FIG. 1.—SIS0 contours superimposed on a $5' \times 5'$ *ROSAT* High Resolution Imager image of η Car. North is to the top, and east to the left. The HRI image has a spatial resolution of about 2″ and shows η Car as a pointlike "core" surrounded by an elliptical limb-brightened "shell" of X-ray emission, immersed in diffuse emission from the Carina Nebula. The point source HDE 303308 is visible about 1′ to the northeast of η Car. The width of the point response function of the SIS means that the SIS spectrum will include contributions from the "core" of η Car, the elliptical "shell," and HDE 303308 (along with diffuse emission from the Carina Nebula).

the High Energy Astrophysics Science Archive Research Center (HEASARC). Figure 1 shows contours of the SIS0 image of η Car superimposed on the *ROSAT* HRI image. The *ROSAT* HRI image shows the "shell" and pointlike "core" of η Car, but such detail cannot be resolved in the *ASCA* image. The X-ray source HDE 303308 (an O3 star about 1′ to the northeast of η Car) is resolved from η Car in the HRI image but is unresolved by *ASCA*.

Figure 2 shows the GIS2 image of the field in the 1–10 keV band. The larger field of view of the GIS reveals a number of additional point sources: the Wolf-Rayet star WR 25 to the southwest of η Car and the cluster Tr 14 to the northwest are most prominent. Figure 3 shows the GIS2 image of the field at energies near the Fe K line at 7 keV. The GIS2 image shows that η Car is the dominant source of emission at these energies, though some weak emission from WR 25 at Fe K is also apparent.

3. THE GIS LIGHT CURVE OF η CAR

In order to determine the level of short-term X-ray variability of η Car during the *ASCA* observation, we extracted a light curve from the screened GIS2 data. We extracted source counts from a circular region of radius 4′.5 centered on the star. We corrected the light curve for background using counts extracted in a source-free circular region of radius 4′.0 centered on a position to the lower left of η Car in the GIS2 detector coordinate image. Because of the nonsymmetric shape of the *ASCA* X-ray Telescope (XRT) + GIS point-source response, background correction can be done only in an approximate manner. However, it is unlikely that incomplete background correction will introduce any spurious variability in the net light curve, since the only known strongly variable X-ray source in the GIS field is η Car. We used a bin size of 1600 s to ensure adequate count statistics. The extracted light curve in GIS2 pulse-height channels 200–850, roughly corresponding to the energy range 2–10 keV, is shown in Figure 4. A linear fit to the 2–10 keV light curve yields $dR/dt = -0.0015 \pm 0.0049$ GIS2 counts s^{-1} day^{-1}. We saw no significant variability from η Car over the duration of the *ASCA* observation.

4. THE *ASCA* SPECTRUM OF η CAR

4.1. *Spectral Extraction*

We extracted spectra from SIS0, SIS1, and GIS2. We did not use the GIS3 data because of a known problem in the conversion from pulse-height (PHA) channels to gain-corrected (PI) channels. We combined data taken in medium and high telemetry rates but excluded all 294 s of low telemetry–rate SIS0 data, since the low-rate data were saturated and produced a spurious excess in the SIS0 spectrum at energies below 2 keV. For the SIS analysis, we used data obtained in "Bright2" mode, i.e., the data were corrected for "echo effect" on an event-by-event basis.

We extracted gain-corrected source and background counts from the GIS2 data using the same extraction regions used to extract the light curve data. For the SIS0 and SIS1 data, we extracted source photons from a $5' \times 5'$ region centered on the source in the SIS detector-coordinate image. The gross count rate from the GIS2 spectrum was 0.753 ± 0.003 counts s^{-1}, while for the SIS0 and SIS1 spectra, the gross rates were 1.036 ± 0.004 and 0.904 ± 0.004 counts s^{-1}, respectively.

Most of the low-energy background is contributed by diffuse emission seen throughout the Carina Nebula (Corcoran et al. 1994a), while the background above 2 keV is dominated by the charged particle–induced events. Both background components can vary across the *ASCA* detectors. To investigate the effects of spatial variations in the background on the derived net spectra, we extracted background spectra from various regions of the SIS0 chip that appeared to be free of source photons. The large point spread of the *ASCA* XRT + SIS means that only relatively restricted portions of the SIS chip are uncontaminated by source photons. We divided the source free region into two subregions: region A (on the lower left of the SIS chip) and region B (on the upper left part of the chip). We then extracted spectra from region A and region B and compared the two. The extracted spectra are shown in Figures 5 and 6.

We modeled the extracted spectra from region A and region B with 2 absorbed Raymond-Smith thermal components with solar abundances, plus an unabsorbed high-energy power-law tail. This is merely a phenomenological model meant to describe the thermal diffuse emission from the Carina Nebula and the nonthermal particle–induced background; a more detailed discussion of the background in the Carina nebula is beyond the scope of this paper. The best fits to the region A and region B spectra are given in Table 2 and are shown in Figures 5 and 6. This model adequately described both the region A and region B spectra, but the derived parameter values do differ somewhat. In particular the 0.5–10.0 keV fluxes differ by about 30%, most of which is contributed by the particle-induced background above 2 keV.

For the SIS0, SIS1, and GIS2 detectors, the background rates, scaled by the ratio of source and background extraction region areas, were 0.075, 0.084, and 0.080 counts s^{-1}.

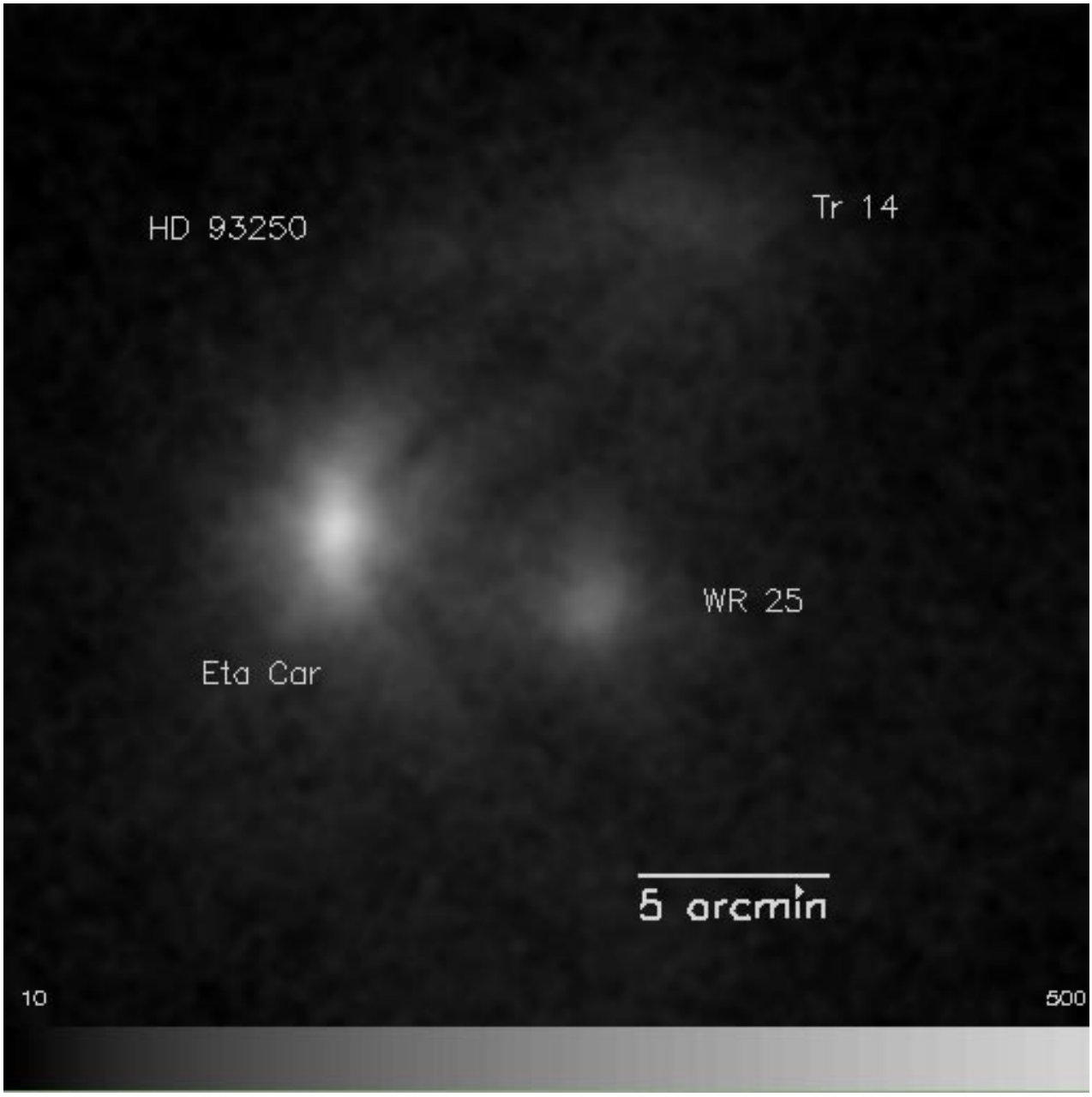

FIG. 2.—GIS2 image of the Carina Nebula near η Car in the 1–10 keV band. North is to the top, and east to the left. η Car is the bright source at the lower left of the image. WR 25 is a fainter source about 7′ to the southwest of η Car, while some emission near the cluster TR 14 and the O3 star HD 93250 to the northwest and northeast, respectively, can be seen. The units of the color scale are GIS2 counts pixel^{-1}.

Thus, the diffuse + particle background contributes only about 10% to the extracted source spectrum. Our modeling of the background spectrum shows that the overall flux variations due to the spatial variation of the diffuse emission are only about 30% of the background, i.e., only about 3% of the overall source spectrum. Thus, the spatial variations of the background should have a negligible effect on our analysis of the net source spectrum.

The neighboring O3 star HDE 303308 could also conceivably contribute to the emission from η Car seen by *ASCA* since *ASCA* cannot resolve this source from η Car. *ROSAT* PSPC observations show that HDE 303308 is a soft X-ray source and so could somewhat contaminate the lowest energy channels in the *ASCA* spectrum. However, the count rate we derive for HDE 303308 from the *ROSAT* HRI data is only 4.4×10^{-3} HRI counts s^{-1}; if the emission is thermal with reasonable spectral parameters ($kT \approx 0.5$ keV and $N_{\rm H} \approx 2 \times 10^{21}$ cm^{-2}), the derived flux is at most only a few $\times 10^{-13}$ ergs cm^{-2} s^{-1} in the 0.1–2 keV band. This is about an order of magnitude lower than the flux from η Car in the same band (see § 4.2 below).

The background-subtracted spectra of η Car from the SIS0, SIS1, and GIS2 data are shown in Figure 7. Strong line emission near the Fe Kα line at 6–7 keV can be easily seen in all spectra, while a peak in the spectrum near 0.5 keV can be seen in both SIS spectra. Note that neither of these features can be seen in the background spectra shown in Figures 5 and 6.

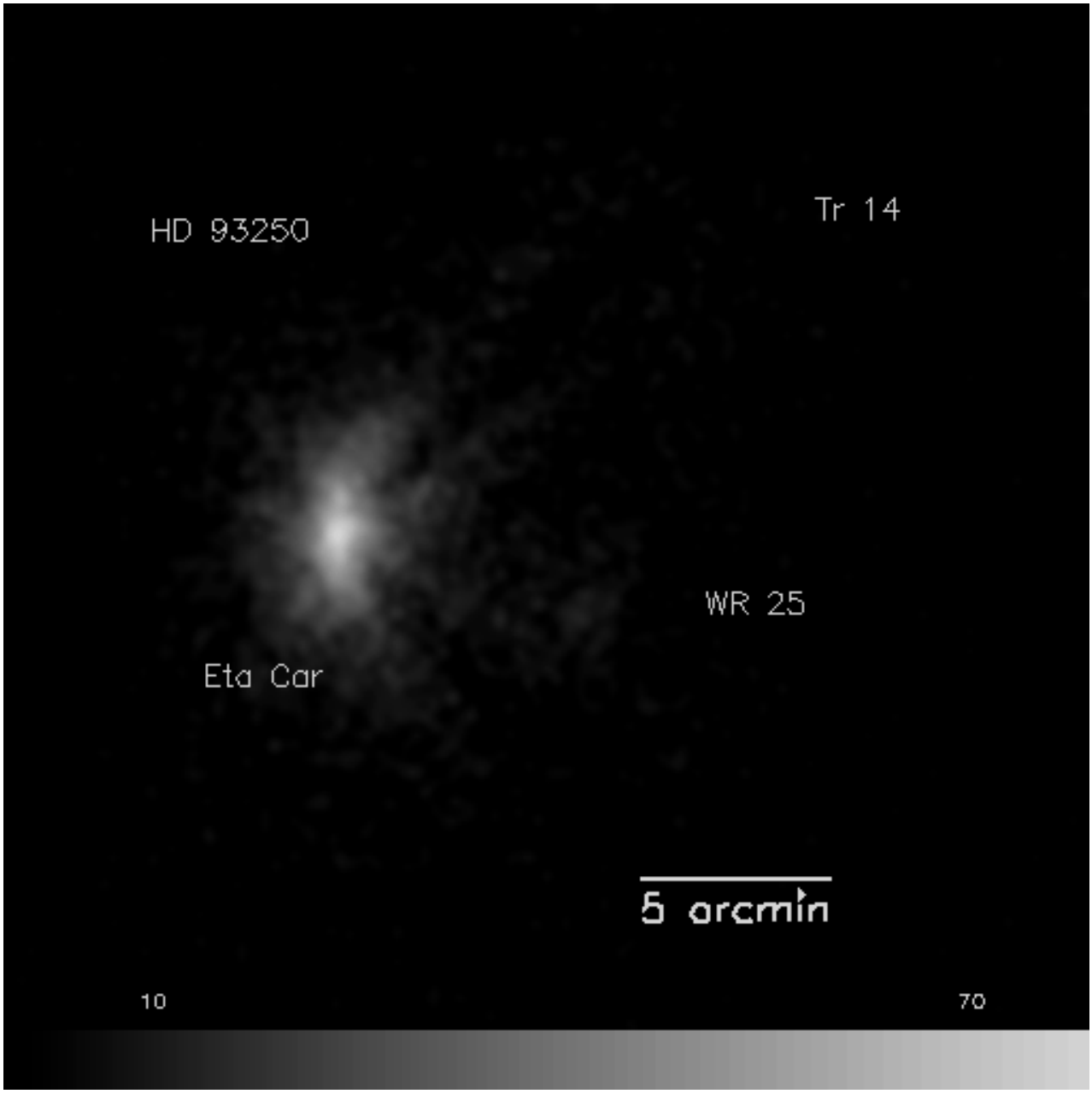

FIG. 3.—GIS2 image in the pulse-height range 530–650, roughly corresponding to the energy range $6.2 \leq E \leq 7.7$ keV, which isolates the Fe K-line emission. Note that η Car provides nearly all the Fe K emission from the region (although some weak emission from WR 25 can also be seen). The units of the color scale are GIS2 counts pixel^{-1}.

4.2. *Spectral Modeling*

We attempted simultaneous modeling of the SIS0 and SIS1 spectra and used the GIS2 spectrum as a consistency check. We corrected all on-axis effective areas to the location of η Car on the CCDs before model fitting. We also rebinned the spectra so that each spectral bin had 10 or more counts. We used a combination of Mewe-Kaastra thermal collisional-equilibrium models (Mewe, Gronenschild, & van den Oord 1985; Mewe, Lemen, & van den Oord 1986; Kaastra 1992; Kaastra & Mewe 1993) with improved Fe-L emission calculations by Liedahl, Osterheld, & Goldstein (1995) using version 9.02 of the XSPEC X-ray spectral modeling software (Arnaud 1996). We used a two-temperature model similar to those of previous X-ray spectral analyses (for example, Chlebowski et al. 1984; CRSP; TKSP). The two thermal components are thought to arise naturally from two distinct emission mechanisms: extended, shocked emission at relatively cool temperatures in the outer "shell," along with much hotter, unresolved shocked emission in the "core" near the central star (Chlebowski et al. 1984; CRSP). We allowed the absorbing column to each thermal component to vary independently and included a fixed interstellar column of 2×10^{21} cm^{-2} (Chlebowski et al. 1984).

4.2.1. *Solar Abundance Models*

We initially tried to fit the *ASCA* spectra using solar abundances (Anders & Grevesse 1989) in emission and

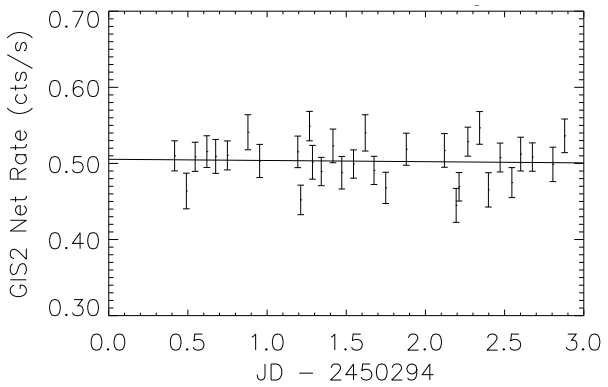

FIG. 4.—GIS2 2–10 keV band light curve. The best-fit straight line is shown.

absorption. The best-fit two-temperature solar model had a value of $\chi^2 = 1989$ using 1077 spectral bins (reduced $\chi^2_\nu = 1.86$) for the SIS0+SIS1 simultaneous fit. The largest residuals occur at energies below 0.7 keV, where the model severely underpredicts the observed spectrum, and at energies near the Fe Kα complex near 6.7 keV. The best-fit solar abundance spectrum is shown in Figure 8, and the derived

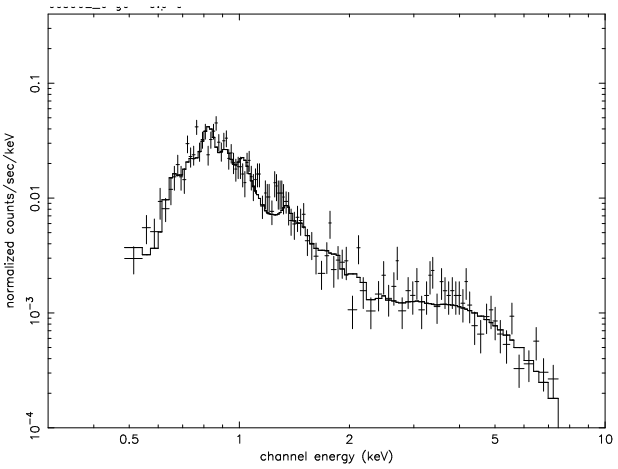

FIG. 5.—SIS0 background from region A with best fit as described in the text.

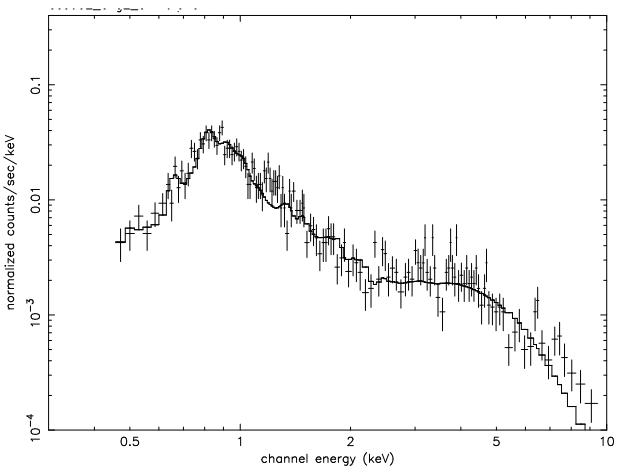

FIG. 6.—SIS0 background from region B with best fit as described in the text.

TABLE 2

MODEL FITS TO SIS BACKGROUND SPECTRA

Parameter [a]	Region A	Region B
log T_1 (K)	6.51	6.40
log EM_1 (cm^{-3})	55.71	55.23
log NH_1 (cm^{-2})	21.45	21.02
log T_2 (keV)	7.05	6.94
log EM_2 (cm^{-3})	54.75	55.01
log NH_2 (cm^{-2})	20.92	20.83
α	0.52	0.44
k	3.08×10^{-5}	4.34×10^{-5}
$L_X/L_\odot$ (0.5–10 keV)	0.31	0.44
χ^2_ν	1.41	1.46

[a] The spectral model consists of two solar abundance Raymond-Smith components plus absorption, with an unabsorbed power law [of the form $A(E) = k(E/1\ \mathrm{keV})^{-\alpha}$] to approximate the effect of charged particle events.

parameters are given in Table 2. The tabulated uncertainties are derived by varying the parameter of interest from its best-fit value and calculating $\Delta\chi^2 = \chi^2_{\mathrm{new}} - \chi^2_{\mathrm{best\text{-}fit}}$; the difference between the best-fit value of the parameter of interest and the value when $\Delta\chi^2 = 2.76$ is taken as an estimate of the formal 1 σ uncertainty of the parameter. Note that these uncertainties are formal statistical errors only and as such represent the precision of the derived parameters. If systematic errors are important, the derived values of the fit parameters will be inaccurate, in the sense that the true parameter value could lie outside the confidence range specified by the tabulated error bars. Systematic errors could arise from three possible causes: (1) an incorrect background correction; (2) an inaccurate instrumental calibration; or (3) an incorrect choice of spectral model. We

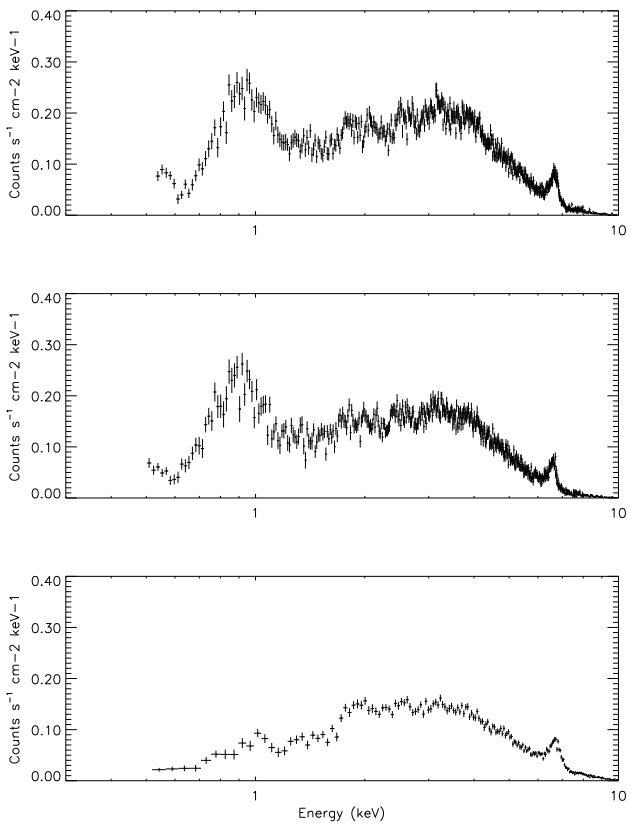

FIG. 7.—SIS0, SIS1, and GIS2 background-corrected spectra

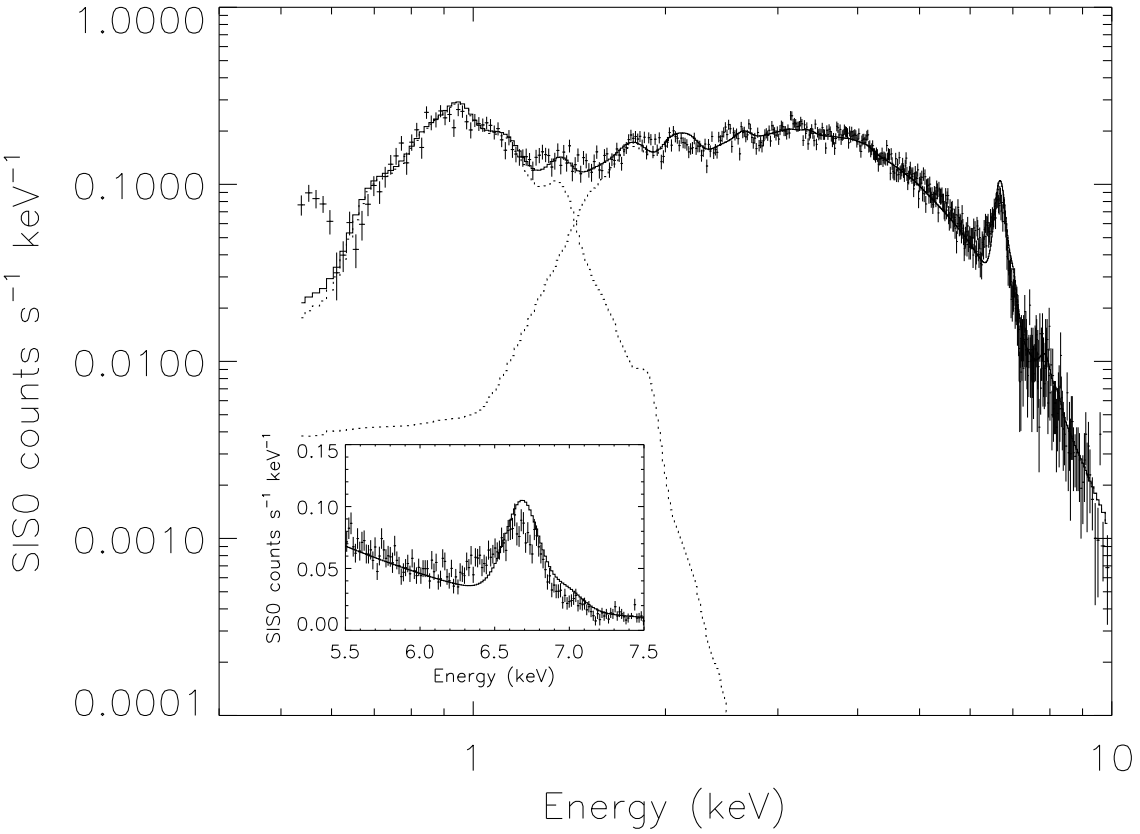

FIG. 8.—Background-corrected SIS0 spectrum of η Car and the best-fit two-temperature solar abundance model. The cool and hot components are shown by dotted lines. The model does not match the observed spectrum at the N blend near 0.5 keV. The inset shows a view of the region near the Fe Kα line. The solar abundance model overpredicts the strength of this line; also, a noticeable excess in the observed spectrum can be seen near 6.4 keV.

believe that systematic errors are small for the following reasons: (1) the extracted spectrum is source, not background, dominated; the extracted background contributes less than 10% of the gross count rate; (2) while there are some known problems in the calibration of the SIS response, these contribute at most only a few percent at restricted energy ranges (mainly near the gold M edge) and typically will not be important except for extremely high signal-to-noise ratio spectra; and (3) the spectral model we chose is very similar to other models derived from analyses of other X-ray spectra of η Car obtained with other X-ray detectors and can be made to fit the data with only minor modifications (see below).

4.2.2. *Nonsolar Abundance Models*

Since η Car is thought to be an evolved star with evidence of nonsolar abundances (Davidson et al. 1995), we tried to improve the residuals by allowing for nonsolar abundances in the emission, similar to the approach used by TKSP. The SIS spectra do not have sufficient resolution to resolve absorption edges clearly, which limits our ability to measure independently abundances in the absorbing material. Since the strongest line features in the η Car X-ray spectrum are due to N, Mg, Si, S, and Fe, we allowed the abundances of these elements in the emission components to vary, while keeping the abundances of the other elements fixed to solar. A better approach would be to take as a starting point the known abundances of η Car as derived from optical or UV spectral analysis. However, we have not adopted this approach, primarily since there is still sufficient uncertainty in the abundances derived from optical and UV spectral analyses for η Car but also because the X-ray emission seen by *ASCA* is a composite of emission originating in spatially distinct regions.

We modeled the SIS spectra varying the abundances of N, Mg, Si, and S for each emission component, assuming the abundances for both components are the same, and using normal solar abundance for the absorbing material and the other elements included in the emission model. Our best fit to the SIS0 and SIS1 spectra using this model improved χ^2 to 1473 with 1077 spectral bins ($\chi^2_\nu = 1.4$). The derived parameters are given in Table 3. We find an overabundance of N similar to that found by TKSP, though the overabundance we find ($N/N_\odot \approx 47$) is much lower than that found by TKSP ($N/N_\odot \approx 210$). Increasing the N abundance primarily increases the strength of the Kα and Kβ lines of helium-like and hydrogen-like N at 0.4–0.5 keV, which in turn increases the brightness of the model at $E \leq 0.6$ keV to match the observed low-energy "excess" in the SIS spectra. We could not match this "excess" by changing the abundance of any other element. Likewise, no such excess at $E \leq 0.6$ keV was visible in any of the extracted background spectra. We also find that Fe is somewhat underabundant, while Mg, Si, and S are slightly overabundant but probably not significantly so. This model is a reasonable description of most of the observed spectrum, except that there is an excess of emission at energies just below the Fe Kα line in both the SIS0 and SIS1 spectra.

4.2.3. *An* Fe *Fluorescence Feature*

We tried to reduce the excess near 6.5 keV by including a Gaussian line in our nonsolar abundance model and refit-

TABLE 3

MODEL PARAMETERS OF BEST FITS TO *ASCA* CYCLE 4 SPECTRA

Parameter	Z = Solar[a]	Z = Nonsolar[b]
log T_1 (K)	6.31 ± 0.04	6.51 ± 0.04
log EM_1 cm^{-3}	58.32 ± 0.09	57.08 ± 0.12
log NH_1 cm^{-2}	21.83 ± 0.03	21.57 ± 0.03
log T_2(K)	7.84 ± 0.04	7.80 ± 0.04
log EM_2 cm^{-3}	57.80 ± 0.01	57.75 ± 0.02
log NH_2 cm^{-2}	22.53 ± 0.01	22.58 ± 0.01
log N/H	−3.95	−2.28 ± 0.09
log Mg/H	−4.42	−4.30 ± 0.09
log Si/H	−4.45	−4.21 ± 0.13
log S/H	−4.79	−4.73 ± 0.07
log Fe/H	−4.33	−4.45 ± 0.01
χ^2_ν	1.86	1.17
$L_X/L_\odot$ (0.5–10 keV)[c]	16.57 ± 0.02	16.27 ± 0.05
$L_X/L_\odot$ (2–10 keV)[c]	15.51 ± 0.02	15.17 ± 0.05
$L_X/L_\odot$ (1.5–2.4 keV)[c]	0.97 ± 0.01	0.96 ± 0.01
$L_X/L_\odot$ (0.5–1.0 keV)[c]	0.43 ± 0.01	0.45 ± 0.01

[a] Solar abundance from Anders & Grevesse 1989.

[b] Abundances of N, Mg, Si, S, and Fe allowed to vary; other elements fixed at solar.

[c] Observed luminosities (i.e., uncorrected for absorption) assuming D = 2.6 kpc

TABLE 4

FLUORESCENT LINE PARAMETERS

Data Set	E_0 (keV)	Equivalent Width (eV)
ASCA Cycle 4	6.44 ± 0.03	126 ± 20
ASCA PV	6.44[a]	≤120

[a] Fixed.

ting. Inclusion of the Gaussian line significantly improved the fit, which resulted in an overall reduction of χ^2 to 1245. The change of χ^2 of 228 from our previous best-fit value means that the line is detected at a confidence ≥99.99%. The derived line parameters are given in Table 4. Figure 9 shows the best fit to the SIS0 data using the two-component, variable abundance model + Gaussian line. The line energy is 6.44 keV, which identifies it as a fluorescent feature produced by photoionization of either neutral or non–highly ionized Fe in the vicinity of the hard X-ray source. This represents the first significant detection of an Fe fluorescent feature in the X-ray spectrum of η Car. The intrinsic spectrum, showing the hot and cool components, the Gaussian line, and the strong N feature near 0.5 keV, is shown in Figure 10.

5. COMPARISON WITH PREVIOUS *ASCA* AND *ROSAT* SPECTRA

Given the greater effective area of *ASCA* at energies above 1.5 keV relative to the *ROSAT* PSPC, the *ASCA* spectrum more tightly constrains the variability of the hard emission reported by CRSP. By comparing the Cycle 4 *ASCA* spectra with the PV *ASCA* observation analyzed by TKSP and the *ROSAT* data analyzed by CRSP, we can determine the level of variability of the hard flux, look for evidence of variability in the soft source, and determine the limits of variation in the temperature and column to the soft and hard components.

5.1. *The PV-Phase ASCA Spectrum*

The *ASCA* PV-phase observation (sequence number 20018000) was made on 1993 August 24–25. We retrieved

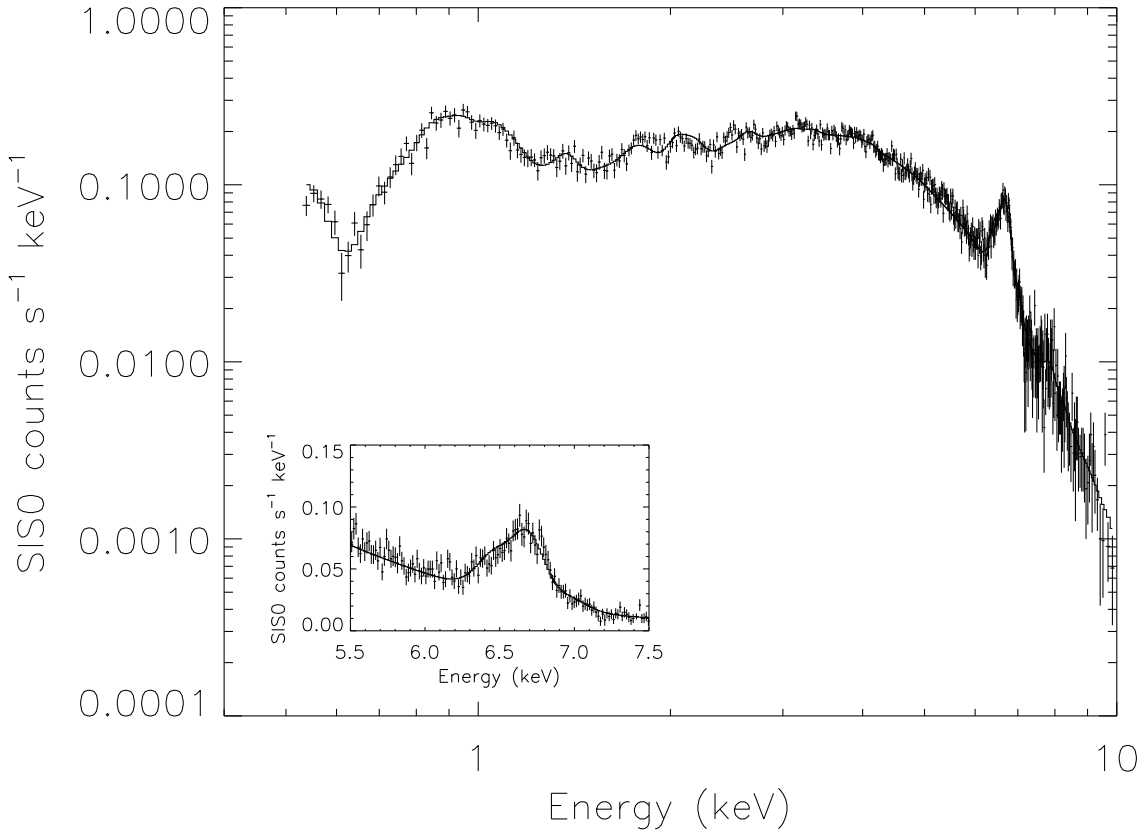

FIG. 9.—Two-temperature variable abundance model fit to the SIS0 spectrum. The model includes a Gaussian line at 6.44 keV and agrees well with the observed Fe K-line profiles, while the excess near 0.5 keV is matched by increasing the strength of the N lines in the model.

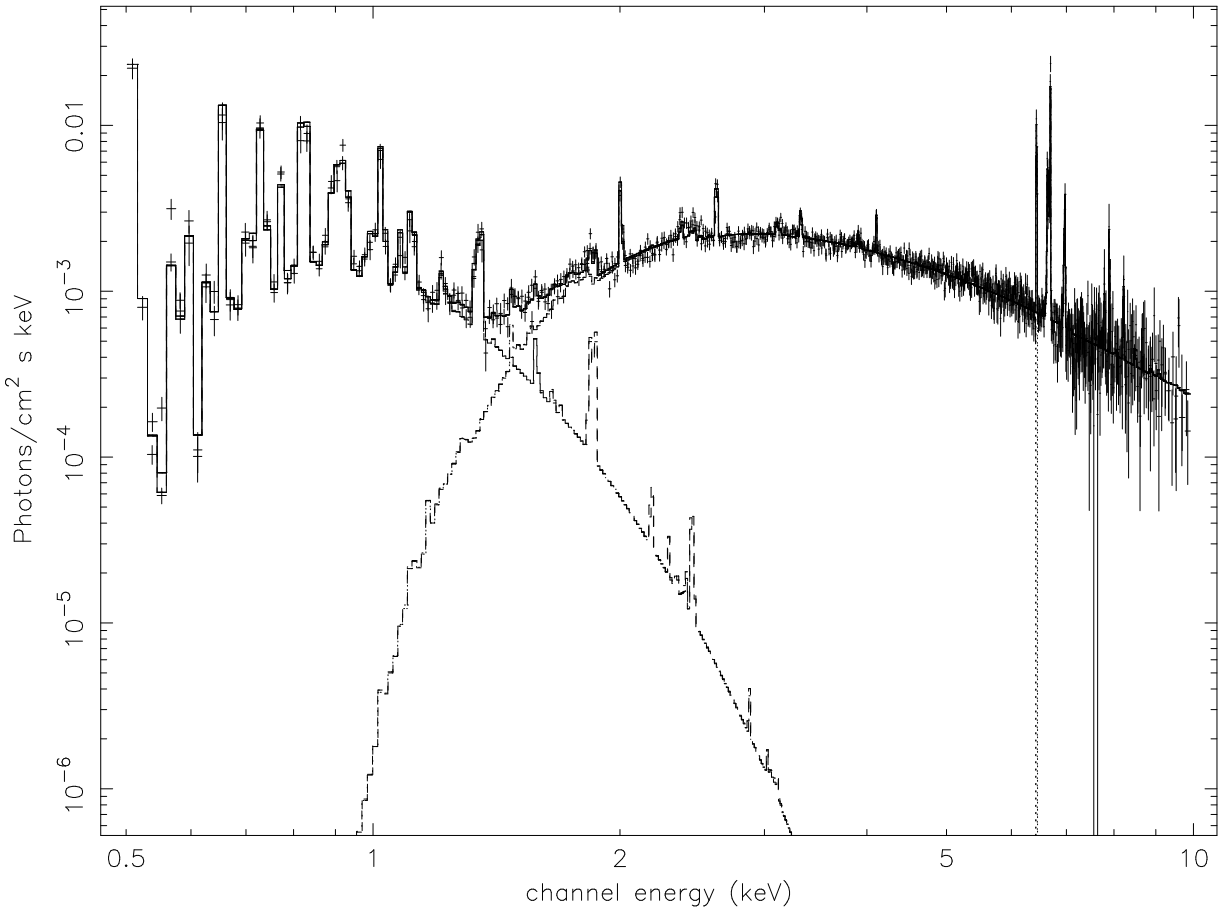

FIG. 10.—Intrinsic two-component nonsolar abundance model. Both thermal components and a variety of emission lines including the N feature near 0.5 keV (a blend of lines dominated by the N VII and N VI Kα and Kβ lines), the Fe line near 6.7 keV, and the narrow Fe resonance line near 6.4 keV are shown.

the raw SIS0 PV-phase data from the *ASCA* archive at the Goddard Space Flight Center. We analyzed only the "Bright" mode data (including "Faint" mode data that were converted to "Bright" mode), since this provided the largest homogeneous data set. We screened the raw data using the same criteria we used to filter the Cycle 4 observation: we excluded times of SAA passage, intervals when the Earth elevation angle was less than 10° (20° for daylit Earth), intervals of low geomagnetic rigidity, and intervals when the pointing deviated more than 0.°01 from the nominal target position. In addition we cleaned the screened SIS0 data for contamination due to "hot" and "flickering" pixels. The filtered SIS0 data had a net exposure time of about 9 ks. This is somewhat lower than the exposure derived by TKSP for the same data set (about 13 ks), since we use a more stringent Earth elevation constraint. We then extracted the source and background spectra from the cleaned SIS0 data, using extraction regions similar to those used in the extraction of the Cycle 4 spectra.

We applied our best-fit two-temperature variable-abundance model described above to the SIS0 PV data. We found we could achieve an acceptable fit to the *ASCA* SIS0 PV data using this model, but in order to fit the spectrum above 2 keV, we needed to reduce the emission measure of the hot component by 2/3. We included the Fe fluorescent feature in the spectrum but found that the PV spectrum could provide only an upper limit to the line strength. Figure 11 shows the best fit to the *ASCA* SIS0 PV data. The parameters of the Fe fluorescent line are given in Table 4, while the overall model parameters for this fit are given in Table 5. Aside from the change in the emission measure, *no significant change in any other parameter was needed.* This confirms the inference of CRSP that the variation in the

TABLE 5

MODEL PARAMETERS OF BEST FITS TO *ASCA* PV AND *ROSAT* SPECTRA

Parameter	*ASCA* PV	*ROSAT*	*ROSAT*
Instrument	SIS0	PSPC	PSPC
Date (UT)	1993 Aug	1992 Dec	1992 Jun
log T_1	6.53 ± 0.08	6.56 ± 0.04	6.61 ± 0.04
log EM_1	56.99 ± 0.22	56.54 ± 0.28	56.44 ± 0.21
log NH_1	21.55 ± 0.14	21.09 ± 1.09	≤ 21.20
log T_2	7.80 ± 0.10	7.80	7.80
log EM_2	57.59 ± 0.04	57.45 ± 0.05	56.67 ± 0.18
log NH_2	22.58 ± 0.02	22.58	22.58
log N/H	-2.28[a]	-2.28	-2.28
log Mg/H	-4.30	-4.30	-4.30
log Si/H	-4.21	-4.21	-4.21
log S/H	-4.73	-4.73	-4.73
log Fe/H	-4.45	-4.45	-4.45
χ^2_ν	1.03	0.74	0.85
$L_X/L_\odot$ (0.5–10 keV)[b]	11.38 ± 0.10	8.45 ± 0.82	2.21 ± 0.42
$L_X/L_\odot$ (2–10 keV)[b]	10.45 ± 0.09	7.76 ± 0.82	1.65 ± 0.42
$L_X/L_\odot$ (1.5–2.4 keV)[b]	0.70 ± 0.01	0.48 ± 0.02	0.11 ± 0.02
$L_X/L_\odot$ (0.5–1.0 keV)[b]	0.41 ± 0.01	0.35 ± 0.12	0.39 ± 0.12

[a] Parameters without error bars were fixed at tabulated value.

[b] Observed luminosities (i.e., uncorrected for absorption) assuming $D = 2.6$ kpc.

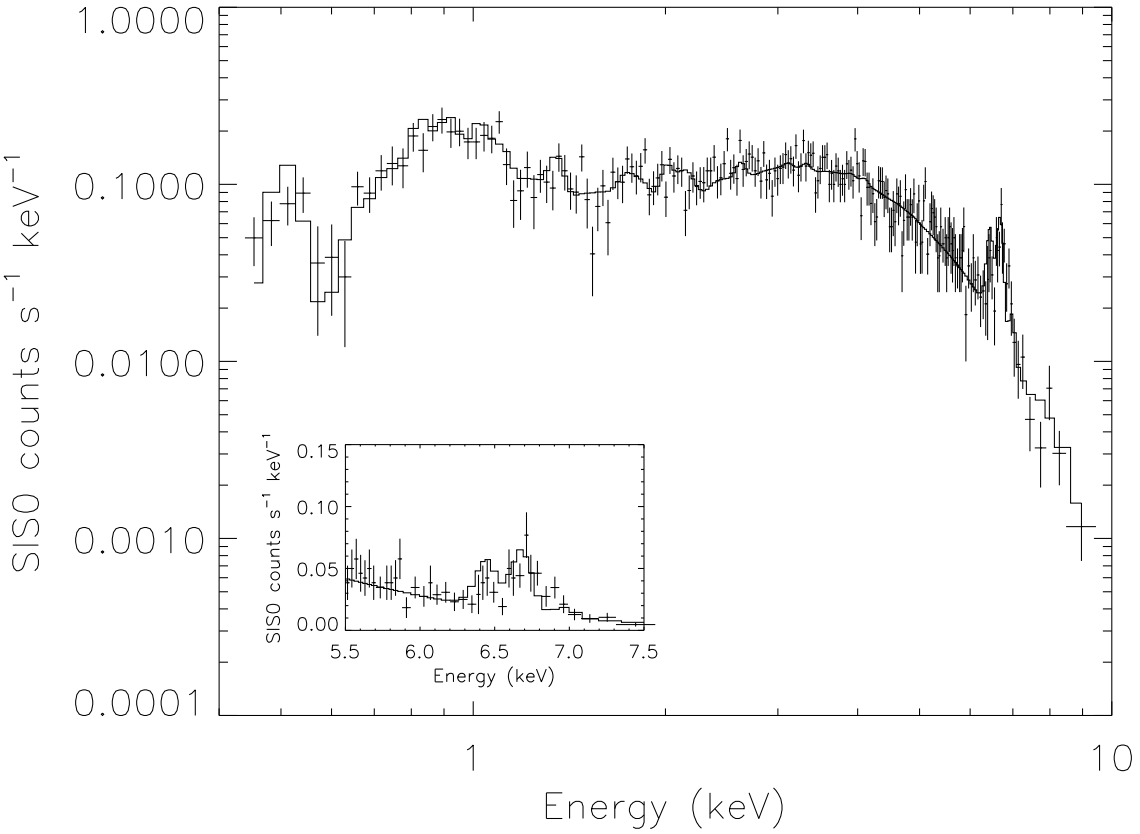

FIG. 11.—SIS0 PV data along with the best-fit two-temperature variable abundance model as described in the text

X-ray flux is confined to a change in the emission measure of the hot component; the temperature of and column depth to that source remain constant.

5.2. *Comparison of the ASCA and ROSAT PSPC Spectra*

We compared the *ASCA* spectral model to the *ROSAT* PSPC spectra analyzed by CRSP. The spectra were from *ROSAT* observations in 1992 June (sequence RP900176N00) and from 1992 December–1993 January (sequence RP900176A01) when the hot component was substantially brighter. We initially tried to fit the *ASCA* variable abundance Mewe-Kaastra model to the *ROSAT* data allowing only the normalization of the hot component to vary. This did not result in an acceptable fit to either of the PSPC data sets, primarily because of significant residuals near 1 keV. In order to generate acceptable fits to both *ROSAT* spectra, we had to vary the soft component emission measure and column density. The parameters for these fits are given in Table 5, and the spectra and best-fit models are shown in Figure 12. Because the emission at $E \leq 1.5$ keV originates in a very extended region, we do not believe the differences in emission measure and column represent a real variation in the soft source between the time of the *ROSAT* and *ASCA* pointings. Rather, it seems more likely that there are residual differences between the *ASCA* and *ROSAT* spectra at low energies, owing to instrumental cross-calibration uncertainties and/or contamination of the *ASCA* spectrum by soft emission that is not present in the *ROSAT* spectra. Real variability of this component would require that a substantial amount of soft emission originates close to the star and that the local absorbing medium is patchy. We point out that the properties of the soft component derived from the two *ASCA* spectra are the same, as are the properties of the soft component derived from the two *ROSAT* spectra, which suggests an instrumental, not cosmic, origin of the spectral differences.

5.3. *X-Ray Variability: 1992–1996*

Tables 3 and 5 show the calculated X-ray luminosities for the four spectra in four bands: the "hard" band (2–10 keV), the "soft band" (0.5–1 keV), the "total" band (0.5–10 keV), along with the "hard *ROSAT*" band (1.5–2.4 keV) used by

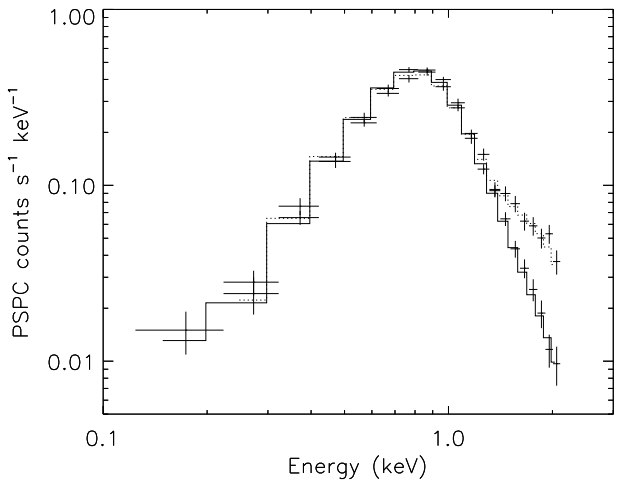

FIG. 12.—*ROSAT* PSPC spectrum from 1992 June and 1992 December and best-fit models as described in text. *Solid line*: best-fit model to the 1992 June spectrum. *Broken line*: best-fit model to the 1992 December–1993 January spectrum. The spectra are nearly identical at $E \leq 1.5$ keV.

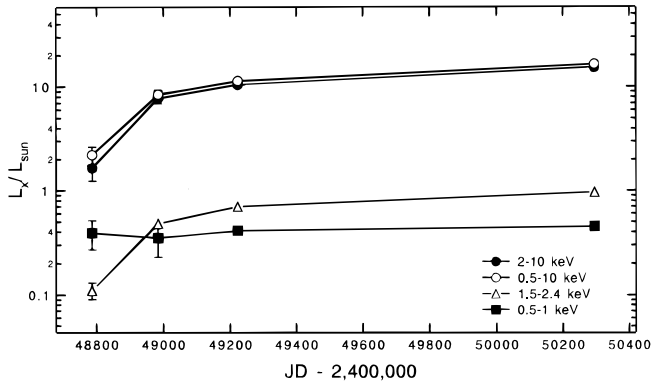

FIG. 13.—X-ray variability of η Car, 1992–1996

CRSP. Note that, since *ROSAT* has no sensitivity at $E \geq 2.5$ keV, the 2–10 keV flux determined from the *ROSAT* observations will only represent the true 2–10 keV flux if the assumed spectral model is correct. The X-ray luminosities are plotted versus Julian Day number in Figure 13. No significant change is seen in the soft band through this period. The hard band flux, however, has increased since 1992 by nearly an order of magnitude and still continues to rise. The rate of increase is not constant and evidently slowed sometime after 1993.

6. ULTRAVIOLET SPECTRAL VARIATIONS

On 1996 July 19, *IUE* observations of η Car were made as a Target-of-Opportunity program in coordination with the *ASCA* observations. The *IUE* spectra were obtained at low and high resolution in the 1200–3200 Å range, using the large entrance aperture (10″ × 20″). Here we limit our analysis to the high-resolution spectra because it allowed us to analyze the different components of the line profiles and to disentangle the serious blending of the rich emission-line spectrum. A more detailed analysis of these data will appear elsewhere. Though emission from the nebula could be a cause of spectral contamination, in fact the observed UV spectrum is thought to be dominated by the emission from the central "core" (Viotti et al. 1989). Casual inspection of the 1996 July *IUE* spectrum of η Car showed it to be very similar to that observed by *IUE* in previous epochs (see, e.g., Viotti et al. 1989). The stellar spectrum is characterized by low- and high-ionization lines, some of which show P Cygni absorptions extending out to velocities of -800 km s^{-1}. As noted by Viotti et al., this suggests that a wide range of ionization exists throughout the wind from the star.

It was recently noted by Damineli et al. (1995) that the star's long-term activity (as depicted by Zanella, Wolf, & Stahl 1984 and Damineli 1996) is marked in the ultraviolet by a large variation of the emission lines of N III] at 1750 Å, Si III] λ1892, the Fe III multiplet at 1895, 1914 and 1926 Å, and the high-excitation Fe II blends at 1785–1788 Å and at 2506–2508 Å. In particular, Damineli et al. found that these features had largely weakened in 1981 July at the time of a shell episode of η Car. Figure 14 compares *IUE* high-resolution spectra near these lines from 1992, 1995, and 1996. These lines have a very complex profile, with broad and narrow emission components that are thought to be formed in different regions of the star's atmospheric envelope. We have found that a significant spectral change took place in 1992 December, when the N III] multiplet and

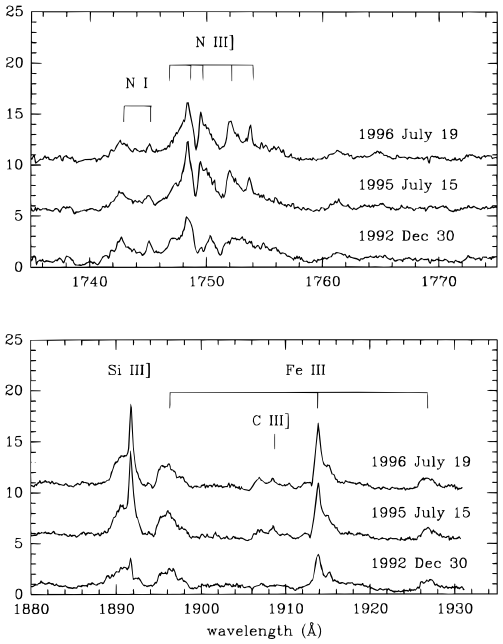

FIG. 14.—Variation of the ultraviolet spectrum of η Car during 1992 December to 1996 July. The N III], Si III], C III], and Fe III emission lines were weaker at the time of the *ASCA* minimum flux and reached a maximum in mid-1995.

the Si III] λ1892, Fe III λ1914 lines were much weaker than in the following years. As shown in Figure 14, this variation was especially evident in the narrow emission components of these lines that in some cases nearly disappeared. No significant change was recorded in the Fe II lines. This minimum in the strengths of these lines is almost certainly associated with the 1992 June episode discovered by Damineli (1996). It should also be noted that the weakening of the Si III] λ1892 and Fe III λ1914 lines occurred at the time of the X-ray brightening reported by CRSP. It is unfortunate that no UV observation of the star was made during the "shell event"/X-ray low state in 1992 June. One year later (1993 December) the line fluxes had nearly recovered to the values observed in the previous spectra, with prominent peaks overlying the strong and broad emission. After this, the fluxes of the N III], Si III], and Fe III lines seem to have further strengthened to reach a maximum in 1995 July, followed by a slight decrease in 1996 July.

Of particular interest is the marked variation displayed by a weak emission line at 1908.5 Å whose wavelength is close to that of the C III] intercombination line. This line was present during 1993–1996 but disappeared in 1992 December. It was also absent in a long-exposure, high-resolution spectrum obtained in 1980 December (described by Viotti et al. 1989). In both cases the *IUE* observations were taken close to a shell episode of η Car, and this fact together with the large variation shown during 1992–1996 by the Si III] line (which should be formed in the same physical conditions) make the identification of C III] quite plausible.

The *IUE* spectrum from the 1992–1996 interval shows that the strengthening of the N III] multiplet, the Si III] λ1892 and Fe III λ1914 lines occurred along with the increase of the hard X-ray component and the observed changes in the metastable 10830 Å emission line of He I described by Damineli (1996). This is suggestive of a struc-

tural change in the outer parts of the expanding envelope of η Car, where the harder X-ray spectrum may also be formed. Alternatively, the apparent correlation between the X-ray emission and the changes in the UV lines could suggest that the change in the X-ray source produces a change in the UV line emission, for example, by a change in the photoionization rate in the outer part of the wind as the X-ray emission changes. Unfortunately, we cannot distinguish between these two scenarios at this time without nearly simultaneous X-ray and UV monitoring.

7. DISCUSSION

7.1. *The Soft X-Ray Emission*

The soft component originates in an extended elliptical "shell" similar in shape to the homunculus, though considerably larger. Observations with the HRI on *Einstein* (Chlebowski et al. 1984) and the *ROSAT* HRI (Corcoran et al. 1996) have provided the best views so far of the morphology of the extended emission and have shown that the emission extends out to 45″ ($\sim$0.6 pc) from η Car in the direction of the W and E condensations (Walborn, Blanco, & Thackeray 1978). As originally suggested by Chlebowski et al., the X-ray emission from the extended source is probably produced by shock heating as material ejected from the star at an earlier epoch collides with the local interstellar medium, similar to the heating of the ISM by supernovae. The temperature in the postshocked zone ($T_{\rm ps}$) is related to the velocity of the expanding shock V_s by $T_{\rm ps} = (3\mu/16k)V_s^2$, where μ is the mean mass per particle and k is the Boltzmann constant. The *ASCA* spectrum yields a temperature for the "shell" material of 3.2×10^6 K. This implies that the velocity of the outward-moving material in the "shell" is 480 km s^{-1}, assuming $\mu = 0.61 m_{\rm H}$ (which is appropriate for a He/H ratio of 0.1). Given the size of the "shell," this material would have to have been ejected from the star more than 1200 yr ago, if the material expanded at constant velocity. If the material in the "shell" has a composition typical of that of luminous blue variables (LBVs), i.e., $X \sim 0.75$ and $Y \sim 0.25$ (Maeder & Meynet 1988), $\mu = 0.94 m_{\rm H}$, and the calculated shock velocity decreases to $V_s \approx$ 390 km s^{-1} while the time of ejection increases to 1500 yr ago. Thus, for any reasonable chemical composition, the event that created the extended X-ray source around the homunculus predates the "Great Eruption" by more than 1000 yr, assuming the material expanded at constant velocity. The derived speed of the X-ray–emitting material in the "shell" is similar to the tangential velocity of 280 km s^{-1} for the west condensation and $\sim$360–600 km s^{-1} for the east condensations as measured astrometrically by Walborn et al. (1978). This suggests that there is very little component of motion for these condensations along the line of sight and that the major axis of the elliptical X-ray–emitting "shell" is nearly in the plane of the sky, if the condensations are the source of the X-ray emission. It is also interesting to note that Walborn, Blanco, & Thackeray derived velocities of 1180 and 1360 km s^{-1} for the NN and NS condensation, which imply an X-ray temperature of $T_{\rm ps} \geq 2.3 \times 10^7$ K near these features. This suggests that there may be a component of the extended "shell" that contributes to the hard emission seen by *ASCA*.

The *ROSAT* HRI image suggests that the thickness of the X-ray "shell" is $\sim$0.15 pc, and thus the total volume of the "shell" is $\sim 10^{54}$ cm^{-3}. The X-ray emission measure of the soft component is EM $\sim 10^{57}$ cm^{-3}, which means that the average density in the "shell" is $n \approx 16$ cm^{-3} and the total mass of X-ray–emitting gas contained in the "shell" is $\sim 0.01\ M_\odot$. The kinetic energy of this material is $\sim 10^{46}$ ergs. For comparison, the total mass of the S condensation alone is thought to be $\sim 0.1\ M_\odot$ (Walborn et al. 1978).

The "local" column density derived from fitting the soft emission is about 4×10^{21} cm^{-2}, in addition to an assumed fixed "interstellar" column of 2×10^{21} cm^{-2}. Assuming $N_{\rm H} = 5.8 \times 10^{21} E_{B-V}$ (Bohlin, Savage, & Drake 1978), the local column corresponds to a "local" reddening of $E_{B-V} \approx 0.7$, in good agreement with the value of the "local" $E_{B-V} = 0.7$ derived by Andriesse et al. (1978).

7.2. *Abundances in the X-Ray–emitting Gas*

The chemical composition of η Car is an important indicator of the evolutionary state of the star, since stellar evolution with mass loss exposes products of core nucleosynthesis at the stellar surface, measurably altering the composition of the outer stellar atmosphere. Most abundance determinations for η Car have generally relied on UV and/or optical spectral analyses (for example, Rodgers & Searle 1967; Davidson et al. 1982, 1986; Viotti et al. 1989). Such analyses may be biased by uncertain knowledge of the ionization balance of the emitting material, which is usually not known very accurately, and by the observed line profiles, which are usually complicated and blended. Since the strongest X-ray line features are K-shell emission lines, ionization balance plays a much smaller role in determining line strength, so in principle abundances determined from strengths of X-ray K-shell emission lines may be more reliable. However, determining chemical abundances from *ASCA* spectra relies on another set of assumptions: that the emitting material is optically thin and in collisional equilibrium, and that the temperature distribution can be reliably determined from the X-ray continuum.

The most important atmospheric chemical tracers of stellar evolution for massive stars are carbon, nitrogen, and oxygen. Both O and N have K-shell lines falling within the *ASCA* energy band; the C K-lines occur near 0.3 keV, below the *ASCA* cutoff. As discussed by Viotti et al. (1989) the large Si III]/C III] intensity ratio seen in the *IUE* spectrum has to be attributed to a low carbon abundance in the η Car ejecta. The overabundance of N suggests a strong nitrogen enrichment relative to oxygen. No obvious line feature near the oxygen K-shell line at 0.65 keV is apparent, which makes an accurate estimate of the oxygen abundance dependent on a reliable fit to the continuum in this region, along with precise modeling of the interstellar and circumstellar O absorption edges. Explicitly fitting the Cycle 4 *ASCA* spectrum for the O abundance yields an abundance within a factor of 2–3 of the solar value. Assuming that the O abundance is not too different from the solar value, we derive an O/N abundance ratio of O/N $\sim$ 0.11 for η Car. It is important to note that this represents the ratio of O/N of the material in the hot gas in the outer part of the homunculus, since photons near 0.5 keV from the "core" region are completely absorbed by the large intervening column of gas and dust.

The O/N ratio we find is much less than the solar value (O/N $\approx$ 7.6; Anders & Grevesse 1989), which indicates substantial enrichment of N relative to O by a factor of nearly 70. Atmospheric enrichment of nitrogen is understood as a

by-product of CNO processing in the core of massive stars. Maeder & Meynet (1988) tabulated stellar evolutionary models for massive stars including convective core overshooting and mass loss, and they show that the surface O/N ratio for a star with an initial mass of 120 $M_\odot$ varies from the cosmic value to a minimum of O/N = 0.02 in the LBV stage at $t \sim 3 \times 10^6$ yr. Given the uncertainty of a factor of 2–3 in the O abundances from the X-ray spectral modeling, our derived value is in fairly good agreement with Maeder & Meynet's model. If the O/N ratio we derive is solely representative of chemical enrichment due to stellar evolution, then this ratio is consistent with a model with an initial mass of 120 $M_\odot$ at an age of about 2.5×10^6 yr. According to Maeder & Meynet, such a star would currently have a mass of about 90 $M_\odot$, a temperature of about 35,000 K, and a luminosity $\log L/L_\odot = 6.4$. Davidson et al. (1982) derived O/N ≤ 0.15 from analysis of ground-based optical and *IUE* UV spectra of a bright condensation in the outer part of the homunculus. This upper limit is consistent with the value we derive. Dust condensation could play a part in optical and UV determinations of the O/N ratio in the outer part of the homunculus, since dust condensation would deplete O relative to N via formation of silicates. Dust should not affect the O/N ratio derived from analysis of the X-ray spectrum, since the temperature of the X-ray–emitting region in the outer part of the homunculus (3.5×10^6 K) is far too hot for dust to survive.

7.3. *The* Fe *Fluorescent Line*

The line we detect at 6.44 keV may arise from any ionization state of Fe below Fe XVIII. The fluorescent line is most probably produced by photoionization of cold or "cool" material (i.e., material at temperatures below X-ray–emitting temperatures) by the hard X-ray source. The equivalent width of the fluorescent line is approximately given by EW $\approx 2.3 N_{24}$ keV, where EW is the equivalent width of the line in keV and N_{24} the total column density of cold material in units of 10^{24} cm^{-2} (Kallman 1995), since the continuum is nearly flat in the line region. The measured equivalent width of the Fe fluorescent line from the Cycle 4 spectrum is 0.12 keV, which yields a column $N = 5 \times 10^{22}$ cm^{-2} of cold material. This is somewhat larger than the column to the hot component ($NH_2 \approx 3.4 \times 10^{22}$) we derived from modeling the *ASCA* Cycle 4 spectrum, but probably not significantly so. This suggests that cool material in front of the hard source, which provides the X-ray absorption, is also the origin of the fluorescent line.

7.4. *Hard X-Ray/UV Variability and the Nature of the Hard Component*

The variable hard component provides most of the clues to an understanding of the emission mechanism and some clues to the underlying physical nature of the star itself. While most massive stars show X-ray emission with temperatures near 1 keV or less, η Car exhibits emission more than a factor of 5 hotter with much higher absorption. The hard component is probably produced via shock heating, but the higher temperatures imply higher shock velocities: $\log T = 7.8$ corresponds to a shock velocity $V_s = 1720$ km s^{-1} (for $\mu = 0.94 m_H$). Chlebowski et al. (1984) suggested a collision between a high velocity stellar wind (with $V \sim 2000$ km s^{-1}) and a stationary dust shell $\sim 10^{16}$ cm from the star as the origin of the hard component. However, while speeds of 2000 km s^{-1} are typical of wind velocities in massive stars, recent work suggests that the stellar wind velocity from η Car is only 500–700 km s^{-1} or so (Lamers 1989; Hillier & Allen 1992). If the wind velocity is really as low as 500–700 km s^{-1}, it would be difficult to generate temperatures as high as 6×10^7 K by a collision between the wind and stationary circumstellar clouds. On the other hand, gas velocities of 1000 km s^{-1} or more have been detected in emission and absorption (Dufour 1989; Damineli et al. 1993), while Viotti et al. (1989) reported the possible detection of a UV line feature with $V \approx 1240$ km s^{-1} associated with the Si IV $\lambda\lambda$1393, 1400 doublet. Thus, it is difficult to completely rule out very high velocity flows near the star.

That the variation in the hard component is not accompanied by a similar change in the temperature of or column to the hard source is a key to the nature of the hard emission. If the hot gas is produced in a shocked region, then the constancy of the temperature implies a constant velocity for the preshock material. If the wind from η Car is involved in this collision, then the shock must occur at a location where the wind velocity is constant, i.e., beyond the wind acceleration zone. The change in the emission measure of the hot material implies that additional hot material has been continually added to the shocked zone since 1992. CRSP suggested an increase in the mass-loss rate to explain the change they saw in the PSPC spectrum. If so, then the mass-loss rate from the central star has continued to increase through the present. If the volume of the hot material is constant, then the change in emission measure corresponds to a change in density of about a factor of 4 from 1992–1996. This could imply a change in the mass-loss rate by a similar factor during this interval. The cause of the increase in the mass-loss rate would need to be explained, of course, but presumably it could be ascribed to a fundamental instability in the atmosphere of the central star. For an object near the Eddington stability limit like η Car, such a speculation is not implausible.

The change in the UV spectral features seems to be correlated with the X-ray variation. If so, then either the change in the X-ray emission drives the change in the UV features (by changing ionization conditions in the wind, for example) or else the mechanism producing the variation in the wind (as measured by the UV line emission) also produces a change in the X-ray–emitting region. Correcting for the absorbing column of 3.8×10^{22} cm^{-2}, the X-ray luminosity of the hard component at the source is $\geq 2.2 \times 10^{35}$ ergs s^{-1} in the 0.5–10 keV band; note that this is a lower limit to the actual X-ray flux at the source, since the large absorbing column to the hard source could hide a substantial amount of soft flux. Still, this is much less than the stellar luminosity, which is $\sim 10^{40}$ ergs s^{-1}.

It is worth noting that the only known class of X-ray–variable massive stars with thermal X-ray spectra are the colliding wind binaries like γ^2 Velorum (Willis, Schild, & Stevens 1995; Stevens et al. 1996) and WR 140 (Pollock 1987; Corcoran 1996). These systems generally consist of a star with a large mass-loss rate (usually a Wolf-Rayet star) and an O-type companion. The X-ray flux from these systems is dominated by the emission from the shocked interface where the winds from the primary and secondary collide. Variations in the emission can be produced as the stars move in their orbits, since the velocity and density at the shock interface changes and/or the observer's line of sight to the shocked gas through the absorbing wind

material changes. In fact, the X-ray spectra of η Car and WR 140 display some qualitative similarities: both show emission at temperatures of a few keV (though the hottest emission from WR 140 is typically 3 keV or so, somewhat cooler than that from η Car) with absorbing columns of 10^{22} or so. The colliding wind model could naturally explain the high-temperature component as a collision between a slow-moving wind from η Car with a fast-moving wind from a less-evolved, massive companion. There are difficulties with such an interpretation, though—mainly that the two best examples of X-ray–emitting colliding wind binaries, WR 140 and γ^2 Vel, show changes in temperature and column (Corcoran 1996; Stevens et al. 1996), unlike η Car. In addition, there is at present no known companion to η Car; however, recently Damineli, Conti, & Lopes (1997) presented evidence that η Car is in fact a single-lined binary system, based on their measures of the radial velocity of the Paγ line. If so, then the colliding wind model will need to be explored further.

8. CONCLUSION

Uniqueness is the main characteristic of η Car, and its X-ray emission is unusual for its temperature distribution, abundance, and absorbing column. The main results of the X-ray analysis presented above are as follows:

1. The X-ray emission of η Car is consistent with a multitemperature spectrum with differing amounts of absorption.
2. Variability of the X-ray emission is confined to a change in the emission measure of the hotter component, which is suggestive of a change in the density (or possibly the geometry) of the emitting region. X-ray variability does not involve measurable changes to the spectral shape of the emission.
3. The X-ray emission is thermal; we find no strong evidence of any type of nonthermal contribution as would be expected from the presence of a collapsed object or strong magnetic fields.
4. Though variable, the X-ray–emitting gas is never out of equilibrium for very long.
5. Observed nonsolar abundances in the X-ray–emitting gas are consistent with the interpretation of η Car as an evolved object, with an initial mass of $\sim 120\ M_\odot$ and a current mass of $\sim 90\ M_\odot$.
6. We detect a fluorescent Fe line at 6.4 keV produced by photoionization of cold or cool material in front of the X-ray source.
7. The velocity of the shock from the extended X-ray source surrounding the homunculus implies a large-scale mass ejection event prior to the "Great Eruption," and comparison of the shock speed to the tangential velocity of nearby condensations suggests that the ejection axis was nearly perpendicular to the line of sight to the star.

One possibility is that the X-ray variability may be the result of a large-scale instability in the photosphere or outer atmosphere of η Car. For example, a large change in the mass-loss rate could provide an increase in the X-ray emission measure and presumably could also account for the variation in emission line strength seen in the UV. On the other hand, a model of the system as a colliding wind binary could also explain the changes in the X-ray emission (and perhaps the UV line profile variations as well). Observations to determine the exact degree of correlation between the change in the X-ray emission, the UV spectrum, and the He I λ10830 line periodicity are required to distinguish between these models.

We are grateful for the help of the *ASCA* staffs at GSFC and ISAS for their aid in acquiring and reducing the *ASCA* data. This paper made use of data obtained from the High Energy Astrophysics Science Archive Research Center (HEASARC) at GSFC. A. D. thanks FAPESP for support. This research has made use of the SIMBAD database, operated at CDS, Strasbourg, France. This research was supported by NASA under contract NAS 5-32490.

REFERENCES

Anders, E., & Grevesse, N. 1989, Geochim. Cosmochim. Acta, 53, 197
Andriesse, C. D., Donn, B. D., & Viotti, R. 1978, MNRAS, 185, 771
Arnaud, K. A. 1996, in ASP Conf. Proc. 101, Astronomical Data Analysis Software and Systems. V, ed. G. H. Jacoby & J. Barnes (San Francisco: ASP), 17
Bohlin, R. C., Savage, B. D., & Drake, J. F. 1978, ApJ, 224, 132
Cassinelli, J. P., & Swank, J. H. 1983, ApJ, 271, 681
Chlebowski, T., Seward, F. D., Swank, J. H., & Szymkowiak, A. E. 1984, ApJ, 281, 665
Corcoran, M. F. 1996, Rev. Mexicana Astron. Astrofis., Ser. de Conf., 5, 54
Corcoran, M. F., et al. 1993, ApJ, 412, 792
———. 1996, in Röntgenstrahlung from the Universe, ed. H. U. Zimmerman, J. Truemper, & H. Yorke (MPE Report 263) (Garching: MPE), 25
Corcoran, M. F., Rawley, G. L., Swank, J. H., & Petre, R. 1995, ApJ, 445, L121 (CRSP)
Corcoran, M. F., Swank, J., Rawley, G., Petre, R., Schmitt, J., & Day, C. 1994a, in AIP Conf. Proc. 313, The Soft X-Ray Cosmos, ed. E. Schlegel & R. Petre (New York: AIP), 159
Corcoran, M. F., et al. 1994b, ApJ, 436, L95
Currie, D. G., et al. 1997, AJ, 112, 1115
Damineli, A. 1996, ApJ, 460, L49
Damineli, A., et al. 1993, A&A, 268, 183
Damineli, A., Cassatella, A., Viotti, R., Baratta, G. B., Carranza, G. J., & Villada, M. 1995, Rev. Mexicana Astron. Astrofis., Ser. de Conf., 2, 41
Damineli, A., Conti, P. S., & Lopes, D. F. 1997, New Astron., 2, 107
Davidson, K. 1987, in Instabilities of Luminous Early Type Stars, ed. H. Lamers & C. de Loore (Dordrecht: Reidel), 127
———. 1989, in Physics of Luminous Blue Variables, ed. K. Davidson, A. Moffat, & H. Lamers (Dordrecht: Kluwer), 101
Davidson, K., Dufour, R. J., Walborn, N. R., & Gull, T. R. 1986, ApJ, 305, 867
Davidson, K., Ebbets, D., Weigelt, G., Humphreys, R. M., Hajian, A. R., Walborn, N. R., & Rosa, M. 1995, AJ, 109, 1784
Davidson, K., Walborn, N. R., & Gull, T. R. 1982, ApJ 254, L47
Drake, S. A., Singh, K. P., White, N. E., & Simon, T. 1994, ApJ, 436, L87
Duncan, R. A., White, S. M., Lim, J., Nelson, G. J., Drake, S. A., & Kundu, M. R. 1995, ApJ, 441, L73
Dufour, R. 1989, Rev. Mexicana Astron. Astrofis., 18, 87
Gaviola, E. 1950, ApJ, 111, 408
Hester, J., et al. 1991, AJ, 102, 654
Hillier, J. D., & Allen, D. A. 1992, A&A, 262, 153
Kallman, T. 1995, ApJ, 455, 603
Kaastra, J. S. 1992, An X-Ray Spectral Code for Optically Thin Plasmas (Internal SRON-Leiden Report, updated version 2.0)
Kaastra, J. S., & Mewe, R. 1993, A&A, 97, 443
Koyama, K., Asaoka, I., Ushimaru, N., Yamauchi, S., & Corbet, R. H. D. 1990, ApJ, 362, 215
Lamers, H. J. G. L. M. 1989, in The Physics of Luminous Blue Variables, ed. K. Davidson, A. F. J. Moffat, & H. J. G. L. M. Lamers (Dordrecht: Kluwer), 135
Liedahl, D. A., Osterheld, A. L., & Goldstein, W. H. 1995, ApJ, 438, L115
Maeder, A., & Meynet, G. 1988, A&A, 76, 411
Mewe, R., Gronenschild, E. H. B. M., & van den Oord, G. H. J. 1985, A&AS, 62, 197
Mewe, R., Lemen, J. R., & van den Oord, G. H. J. 1986, A&A, 65, 511
Morse, J. 1996, Sky & Tel., 92(4), 13
Pollock, A. M. T. P. 1987, A&A, 171, 135
Raymond, J. C., & Smith, B. W. 1977, ApJS, 35, 290
Rodgers, A. W., & Searle, L. 1967, MNRAS, 135, 99
Serlemitsos, P., et al. 1995, PASJ, 48, 171
Seward, F. D., & Chlebowski, T. 1982, ApJ, 256, 530
Seward, F. D., et al. 1979, ApJ, 234, L55
Smith, M. A., Murakami, T., Ezuka, H., Anandarao, B. G., Chakraborty, A., Corcoran, M. F., & Hirata, R. 1997, ApJ, 481, 479
Stevens, I. R., Corcoran, M. F., Willis, A. J., Skinner, S. L., Pollock, A. M. T., Nagase, F., & Koyama, K. 1996, MNRAS, 283, 589

Tanaka, Y., Inoue, H., & Holt, S. S. 1994, PASJ, 46, L37
Tsuboi, Y., Koyama, K., Sakano, M., & Petre, R. 1997, PASJ, 49, 85 (TKSP)
van Genderen, A. M., & Thè, P. S. 1984, Space Sci. Rev., 39, 317
Viotti, R., Rossi, L., Cassatella, A., Altamore, A., & Baratta, G. B. 1989, ApJS, 71, 983
Walborn, N. R. 1976, ApJ, 204, L17
Walborn, N. R., Blanco, B. M., & Thackeray, A. D. 1978, ApJ, 219, 498
Willis, A. J., Schild, H., & Stevens, I. R. 1995, A&A, 298, 549
Zanella, R., Wolf, B., & Stahl, O. 1984, A&A, 137, 79